Synthesis of double network nanohydrogel and its performance in release of doxorubicin

Ghasem Rezanejad Bardajee[1), 2) *)] (ORCID ID:0000-0001-7331-0059)**, Maede Noruzian**[1)] (0009-0002-3896-4027)**,
Khadijed Didehban**[1)] (0001-0001-5158-0891)

Abstract: The synthesis, properties, and performance of a controlled drug (doxorubicin, DOX) release system based on a double-network nanohydrogel (DNN) obtained from poly(acrylic acid) grafted onto sodium alginate (S-ALG) are described. The drug release behavior of DNNs was studied under different pH and temperature conditions. The DNNs were characterized by ultraviolet-visible (UV) spectroscopy, scanning electron microscopy (SEM), Fourier transform infrared spectroscopy (FT-IR), dynamic light scattering (DLS), and thermogravimetric analysis (TGA). DNN was confirmed to be suitable for use in controlled drug delivery systems.

Keywords: nanohydrogel, double network gel, drug release, poly(acrylic acid), doxorubicin.

Synteza nanohydrożelu o podwójnej sieci i jego działanie w uwalnianiu doksorubicyny

Streszczenie: Opisano syntezę, właściwości i wydajność systemu kontrolowanego uwalniania leku (doksorubicyny, DOX) opartego na nanohydrożelu o podwójnej sieci (DNN), otrzymanego z poli(kwasu akrylowego) szczepionego na alginianie sodu (S-ALG). Zachowanie DNN podczas uwalniania leku badano w różnych warunkach pH i temperatury. DNN scharakteryzowano za pomocą spektroskopii w nadfiolecie widzialnym (UV), skaningowej mikroskopii elektronowej (SEM), spektroskopii w podczerwieni z transformacją Fouriera (FT-IR), dynamicznego rozpraszania światła (DLS) i analizy termograwimetrycznej (TGA). Potwierdzono, że DNN nadaje się do stosowania w systemach kontrolowanego dostarczania leków.

Słowa kluczowe: nanohydrożel, żel o podwójnej siatce, uwalnianie leku, poli(kwas akrylowy), doksorubicyna.

Nanohydrogels are highly physically or chemically cross-linked nano-sized hydrogel systems that could be used to improve drug encapsulation [1, 2]. Nanohydrogels are three dimensional hydrophilic networks with a high absorption capacity for water or aqueous solutions. The researchers are interested in nanohydrogels as a favorable and innovative drug delivery system [3–5].

S-ALG (alginate) is an anionic biopolymer with characteristics such as high solubility in water, the tendency to form a high porosity gel under suitable conditions, biocompatibility, and non-toxicity. In general, drug carriers with the structure of hydrogel nanoparticles are synthesized through the addition of counter ions to alginate to form cross-links and subsequently interlayer networks.

Although any cation can initiate the reaction, most researchers prefer Ca²⁺. When different anti-tuberculosis drugs are compared in free form and encapsulated in alginate nanoparticles, it becomes clear that all of the encapsulated drugs have substantially better bioavailability than the free drugs [6, 7].

DOX (doxorubicin) is helpful in the treatment of many different types of cancer, including breast, uterine, ovarian, lung and cervical. It is a significant drug that can be used to treat cancer [8–10].

Nanocarriers such as nanohydrogels, which are biocompatible, and biodegradable increase the effectiveness of DOX by preventing its degradation in the body. They have demonstrated an approach with low toxicity and good biocompatibility in drug delivery systems [11, 12].

Hydrogel-based drug delivery has attracted the attention of scientists. Hydrogels can protect the drug against aggressive environmental factors such as enzymes or pH changes. The porosity of the hydrogels causes the drug to be loaded into the gel matrix and released at a predetermined rate [13, 14].

[1)] Department of Chemistry, Payame Noor University, PO BOX 19395-3697, Tehran, Iran.
[2)] Department of Polymer and Materials Chemistry, Faculty of Chemistry and Petroleum Sciences, Shahid Beheshti University, 19839-63113, Tehran, Iran.
[*)] Author for correspondence: rezanejad@pun.ac.ir
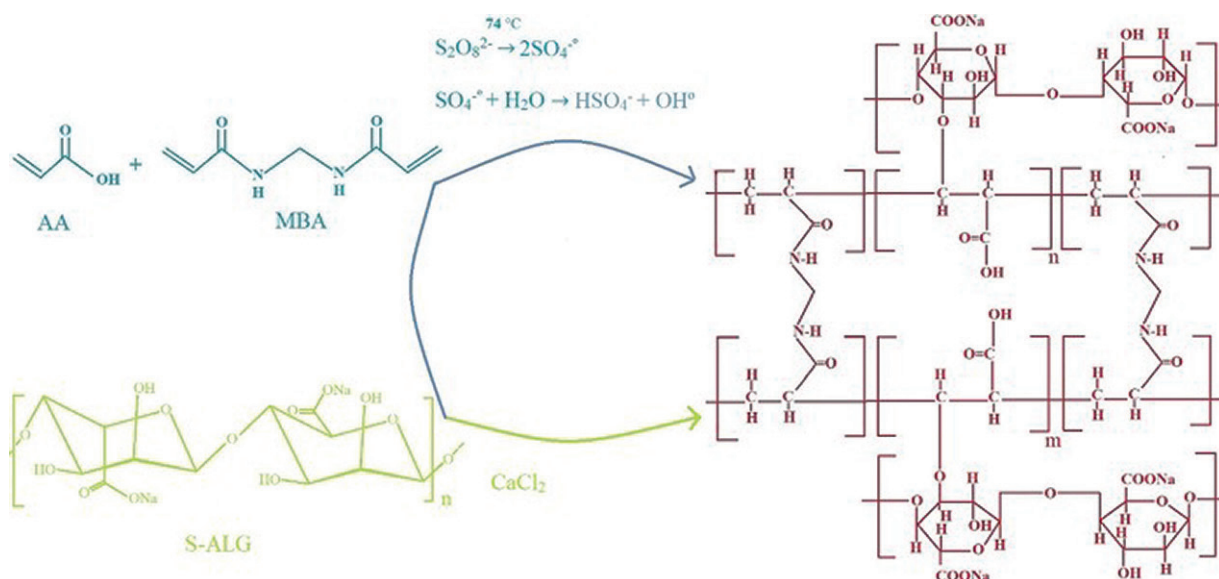
Scheme 1. The mechanism for the formation of DNN

Since the earliest research on double network hydrogels was accomplished 20 years ago, they have flourished as innovative soft materials. Compared to double network hydrogels, single network hydrogels have weak mechanical properties. To overcome the limitations of single network hydrogels in mechanical properties, two unique opposing network structures in double network hydrogels were formed [15-17]. The cross-linking of two networks can be formed and adjusted through chemical cross-linking, physical/chemical cross-linking, and physical cross-linking [18], Therefore, double network hydrogels are better candidates for energy, environmental, and medical applications due to their remarkable mechanical properties, excellent hydrophilicity, rapid self-healing, high conductivity, and rapid stimulus response [15, 19–22].

In 2022, Surikutchi *et al*. developed a hydrogel loaded with nanocapsules for intraperitoneal (IP) drug delivery. Thiol-maleimide and poly(ethylene glycol) are used to make the hydrogel. Nanocapsule-loaded poly(ethylene glycol) gels can find potential applications as biodegradable drug delivery systems that can be implanted in the peritoneal cavity, for example, at the site of tumor resection to prevent the recurrence of microscopic tumors [23].

In 2023, Zhang *et al*. reviewed the recent development of polysaccharide-based double network hydrogels, which show many advantages in mechanical, physicochemical, biocompatibility, and biodegradability properties. The preparation, structure, and unique properties of various polysaccharide-based double network hydrogels are discussed in detail and, in this research, the applications of polysaccharide-based double network hydrogels in the fields of energy storage and conversion and biomedicine are summarized [24].

In 2021, Zeng *et al*. designed a DNN (double network nanohydrogels) that demonstrated pH responsiveness, excellent cold resistance, and efficient recovery at a low temperature of -20°C. Using lomustine as an experimental model, the results of biocompatibility and sustained drug release behavior demonstrate that PAAm/Alg-Ca based DNN paves the way for the development of anticancer drugs cryopreservation and delivery vehicle [25].

In the present study, DNNs were synthesized with a one-pot procedure in water/oil emulsion media by inverse miniemulsion polymerization. Aqueous droplets (containing polymerizable monomers, initiator molecules, and cross-linker molecules) were dispersed in a non-polar liquid (oil phase) for obtaining an inverse miniemulsion. The $CaCl_2$ particles, as a cross-linking agent (in inverse miniemulsion polymerization), migrate to the emulsion droplet interface, where they dissolve into the aqueous phase to produce Ca^{2+} ions for S-ALG chain cross-linking. The process of converting micro/nano monomer droplets into micro/nano polymer particles (in heterophase polymerization) is known as the miniemulsion technique [26, 27]. DOX, as a drug model, was loaded into the substrate of DNNs synthesized from AA grafted on the biopolymer chain of S-ALG. The concentration of AA, MBA, and APS was optimized to produce a better DNN. Then, to confirm the successful synthesis of DNNs, FT-IR, SEM, DLS, and TGA methods were used for characterization. DOX was entrapped and released using DNN as a carrier. To demonstrate the advantages of DNN in the drug delivery system over single network nanohydrogel (SNN), authors synthesized SNN and compared it with DNN. UV spectroscopy was used to examine the swelling capacity. The drug was loaded and released under various environmental conditions, including temperature and pH. In the scheme 1 the general reaction is presented.

EXPERIMENTAL PART

Materials

Ammonium peroxodisulfate (APS, 97%) was purchased from Riedel-de Haën (Honeywell, Charlotte, NC, USA) for the preparation of DNNs. Calcium chloride

dihydrate (99%), *N,N'*-methylenebisacrylamide (MBA), sodium alginate (S-ALG), acrylic acid (AA, 99%), n-hexane (99%), toluene (99%) and ethanol (99%) were purchased from Merck (Darmstadt, Germany). DOX was obtained from Actoverco (Baharestan Industrial Town, Karaj, Iran). Span© 80 (sorbitan monooleate), a yellow liquid with a hydroxyl value of 190-210 and a saponification value of 145-160, and tween© 80, a light-yellow viscose liquid and a non-ionic surfactant with a viscosity of 400–500 cSt at 25°C and a saponification value of 45–55. Both were purchased from Loba Chemie (Colaba, Mumbai, India). All chemicals were of reagent grade and used as received without further purification.

Methods

Field emission scanning electron microscopy (MIRA FEG-SEM, Tescan, Czech Republic) was used to examine the morphology of obtained samples. FT-IR spectra were obtained with a Bruker Tensor 27 spectrometer (Billerica, MA, USA). The TGA of nanohydrogels was performed with a Perkin-Elmer Pyris Diamond DSC (Shelton, CT, USA). TGA/DTG was performed under N_2 at a heating rate of 10°C/min. Size distribution of nanohydrogels was measured by the NANO-flex® 180° DLS system (Colloid Metrix, Meerbush, Germany). A PG instrument T80+ UV–visible spectrophotometer (PG Instruments Ltd., Leicestershire, United Kingdom) was used for recording absorption spectra in solutions.

Synthesis of DNN

For the preparation of the aqueous phase, 16.7 µl APS 2.5% (w/v) as a radical polymerization initiator, 13.2 µl MBA solution 2.5% (w/v) as a cross-linking agent, 120 µl AA as a monomer and 100 µl S-ALG solution 1% (w/v) were added to the micro tube on the vortex stirrer [28].

To prepare the first organic phase, 0.68 g of span© 80 (as a lipophilic surfactant) and 0.52 g of tween© 80 (as
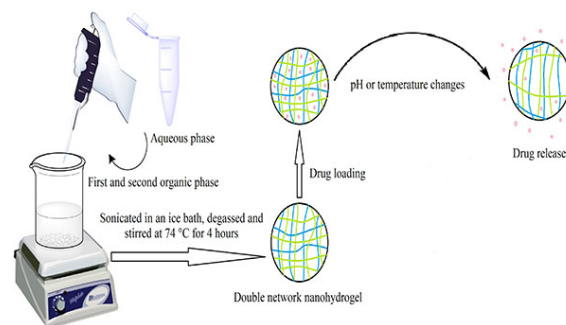

Fig. 1. The preparation of DNN and drug release conditions

a hydrophilic surfactant) [29] were added to 10 mL of n-hexane then the mixture was homogenized for 5 min.

To prepare the second organic phase, 3 mL tween© 80 was mixed with 48 mL toluene and the mixture was stirred for 5 min. Then 6 mL of 0.1 M $CaCl_2$ solution prepared in ethanol. Obtained solution was stirred for 10 min. The reaction mixture was sonicated for 15 min, and then the reaction container was placed in an oil bath at 75°C for 2 hours to evaporate ethanol.

10 mL of the first organic phase and 5 ml of the second organic phase were added to the container under the homogenizer, and then the 3 ml of aqueous phase was slowly added to the reaction mixture and stirred for 10 min. After that time, the reaction container was sonicated in an ice bath for 15 min, and it was degassed with helium and stirred at 74°C for 4 hours. The mixture was centrifuged (7000 rpm, 25 min) with ethanol (20 wt%) and the resulting white powder was dried for 12 hours at 35°C (to keep the structure of DNN) in an oven under vacuum.

Compared to the previous work (preparation of a bulky double network hydrogel with a conventional radical polymerization technique) [30], in this study, DNN particles were synthesized in nanodimensions with the inverse miniemulsion polymerization technique. The general reaction preparation of DNN and drug release conditions is shown in Figure. 1. Compared to single network hydrogels, the flexibility of DNNs is due to the existence of more
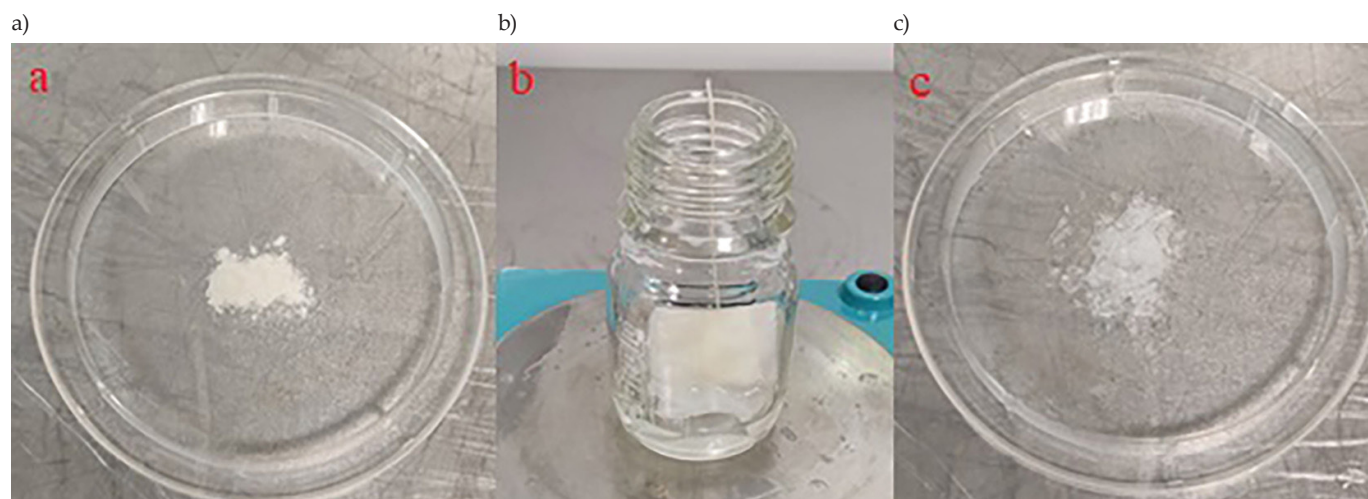
a)   b)   c)

Fig. 2. Water absorption process: a) dry DNN powder, b) water absorption stage, c) swollen DNN

a)

b)

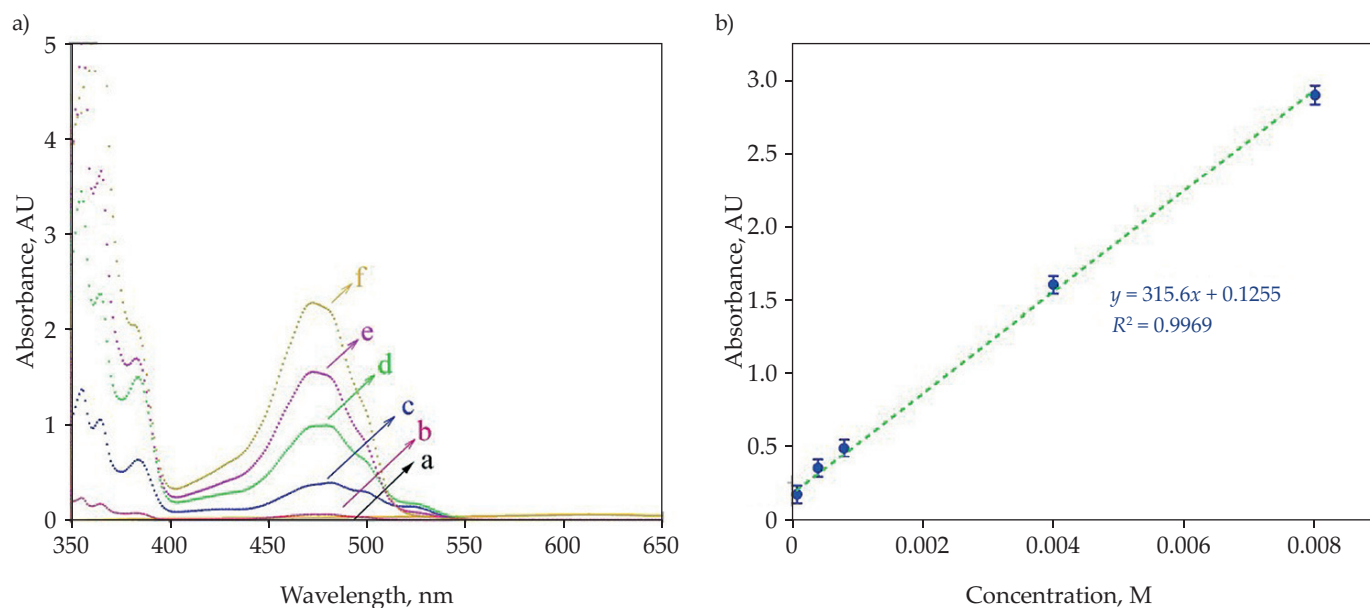$y = 315.6x + 0.1255$
$R^2 = 0.9969$

Fig. 3. a) absorption of DOX standard samples, b) calibration curve of DOX standard samples

cross-linking in them. For this reason, DNNs show better stability than single network hydrogels [31].

Synthesis of SNN

SNNs were obtained using the synthesis method described previously, and they were compared with DNNs. Although SNN was synthesized without the use of $CaCl_2$ (a cross-linker), all the procedures were like those of DNN.

Water absorbency

As shown in Fig. 2, 0.05 g of dry DNN powder was placed in tea bags and completely immersed in 10 mL of distilled water for 3 hours. Then, the equilibrium swelling capacity (ES) was measured at room temperature using Equation 1:

$$ES(g/g) = \frac{W_2 - W_1}{W_1} \qquad (1)$$

where W_1 and W_2 are the weights of dry and swollen nanohydrogels, respectively [32].

Drug loading

1.5 mL of DOX solution (8×10^{-3} M) was added to 0.05 g of the synthesized DNN in a container, and the mixture was stirred for 24 hours. Then it was centrifuged for 20 min at 7000 rpm to separate the drug-carrying polymer. Then the drug loaded DNN was dried for 8 hours at 35°C to preserve the structure of DNN (in an oven operating under vacuum) [32–34]. The drug loading content (DL) was calculated from Equation 2:

$$DL = \frac{D_2 - D_1}{D_1} \cdot 100 \qquad (2)$$

where D_1 and D_2 are the weights of dry nanohydrogel, and drug loaded nanohydrogel, respectively. According to this equation, DL was 18.1%.

Drug release

To determine the amount of drug released by the spectrophotometer UV-Vis (485 nm), phosphate buffer solutions (PBS) were prepared with different pH values (5.4, 7.4, and 9.0). The DOX loaded DNN was placed in the buffer solution in bag-like tea bags. The container was stirred, and samples of the solution containing the released drug were taken at specific times. At regular time intervals, a defined amount of the buffer was separated and replaced with a freshly preheated PBS. The calibration curve at 485 nm was obtained in Fig. 3b, based on the absorption curve of the DOX standard samples (Fig. 3a, Table 1). The amount of drug release was calculated at different concentrations using the calibration curve [32].

T a b l e 1. Absorption of DOX standard samples according to concentration

Samples	1	2	3	4	5	6
Concentration, M	0	$8 \cdot 10^{-5}$	$4 \cdot 10^{-4}$	$8 \cdot 10^{-4}$	$4 \cdot 10^{-3}$	$8 \cdot 10^{-3}$
Absorbance, a.u.	0	0.1	0.3	0.4	1.4	2.6

RESULTS AND DISCUSSION

Characterization

The final swelling capacity of the DNN can be affected by various factors. Therefore, the concentration of components such as AA, MBA and APS was optimized in this study to achieve a better product [32, 35]. The effect

a)

b)

c)
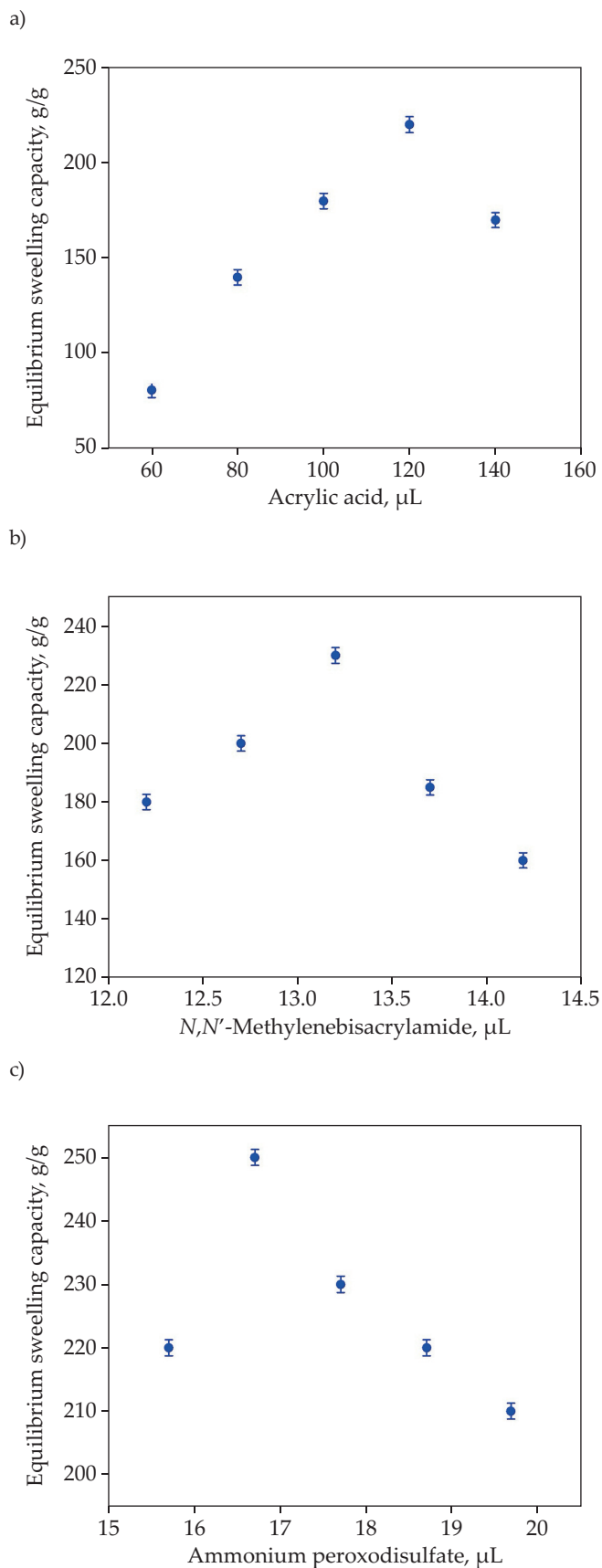
Fig. 4. Effect on equilibrium swelling capacity of the DNN: a) AA, b) MBA, c) APS

of AA on the water absorption of the synthesized DNNs is displayed in Fig. 4a. 60, 80, 100, 120 and 140 μl of AA were used, where the maximum swelling was obtained at 120 μl of AA. As shown in Fig. 4a, with the increase in monomer concentration, the swelling of the nanohydrogels grows initially, which results in more water absorption. If the concentration of monomer in the surrounding medium is higher than what is considered optimal, the swelling of the nanohydrogel will decrease because the high viscosity of the environment will prevent the movement of free radicals and monomer molecules [32]. As the viscosity increases, it becomes more difficult for free radicals to access monomers, which improves cross-linking and reduces DNN swelling (due to fewer spaces available for water absorption). Also, the DNN swelling is appropriate in an optimal ratio between S-ALG and monomer, and when this ratio is disturbed, the DNN swelling decreases.

Cross-linking density is an important factor in DNN water absorption, thus the effect of various concentrations of MBA on DNN water absorption was investigated to determine the optimal concentration. The maximum absorption was obtained at 13.2 μl (2.5% w/v) of MBA, as shown in Fig. 4b. The increase in cross-linking of polymer chains and the reduction of free space between them is caused by the high concentration of MBA, which prevents further expansion of DNN from holding a large amount of water [36, 37].

The initiator concentration (APS) was investigated because it is also swelling capacity factor. Like the previous two factors, initially the water absorption increases with the enhancement of initiator concentration until 16.7 μl (2.5% w/v) of APS, and then it decreases with the increase of APS concentration. As shown in Fig. 4c, an increment in the number of free radicals leads to an initial rise in water absorption. The decrease in water absorption capacity after the optimum point (16.7 μl of APS) can be explained based on the rise in the importance of the end-stage reaction by bimolecular collisions [38–40].

Based on the obtained results, the maximum water absorbency under the following optimization conditions was determined to be 250 g/g: 120 μl of AA, 13.2 μl (2.5% w/v) of MBA, and 16.7 μl (2.5% w/v) of APS [32].

The hydrogel swelling behavior is important to understand, because drug release in hydrogels is based on the swelling behavior in different environments, and a swollen hydrogel facilitates drug diffusion by creating a hydrated environment [41]. Hydrogel swelling kinetics, the water absorption capacity of SNN and DNN in distilled water at different time intervals is shown in Fig. 5a. The rate of water absorption by SNN and DNN decreased over time. DNN reached swelling equilibrium after 90 min (250 g/g) and SNN after 110 min (112 g/g), while in the previous study for bulk double network hydrogel of poly(acrylic acid) grafted onto S-ALG, as a non-nanogel system, equilibrium swelling was reached after 400 min
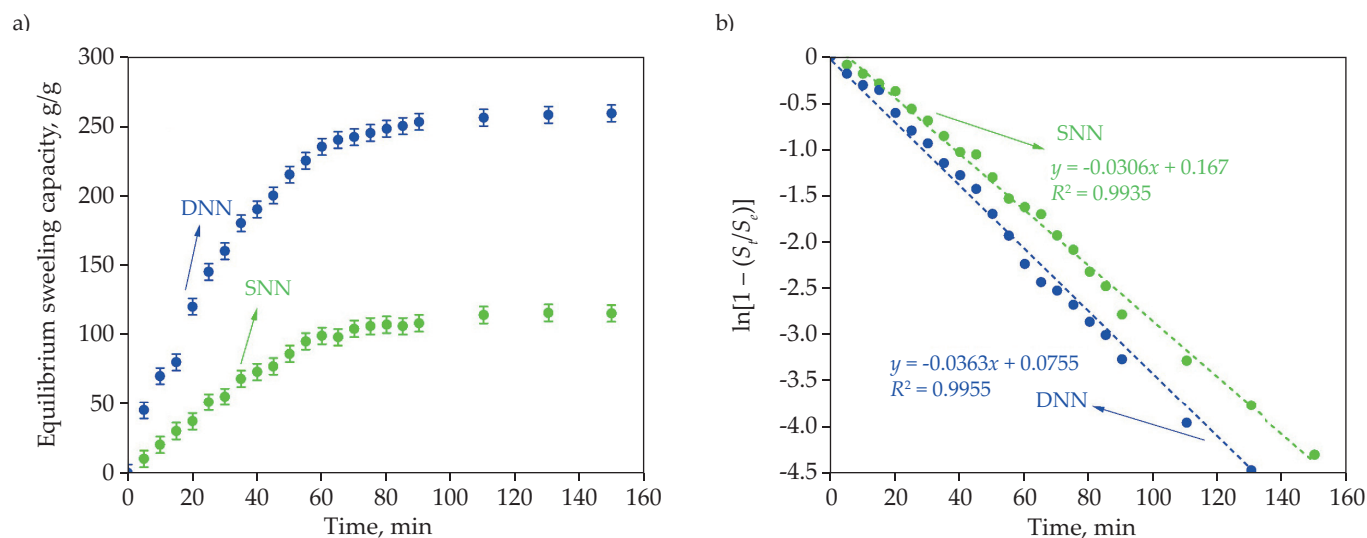
a)

b)

Fig. 5. a) water absorption equilibrium capacity of DNN and SNN, b) ln [1 – (S_t/S_e)] versus time plot for the swelling of DNN and SNN
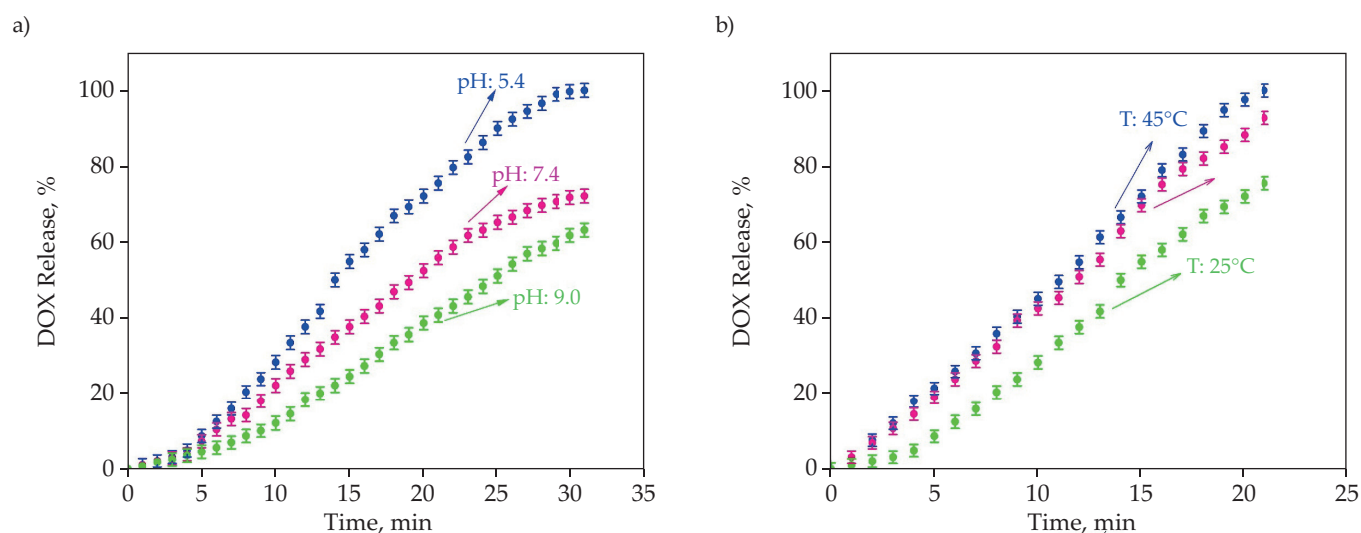
a)

b)

Fig. 6. DOX release from DNN in PBS: a) different pHs at 25°C, b) different temperatures and pH 5.4

(90 g/g) [30]. Swelling time was calculated according to Equation 3 (Voigt-based equation):

$$S_t = S_e(1 - e^{-t/\tau}) \qquad (3)$$

where S_t is the swelling at time (g/g), S_e is the equilibrium swelling (g/g), t is the swelling time (min), and τ (min) is the rate parameter (the τ value is a measure of swelling rate) [42, 43].

After rearranging the Eq. 3, Equation 4 was obtained:

$$-t / \tau = \ln [1 - (S_t/S_e)] \qquad (4)$$

Based on this formula, the rate parameter is obtained as a function of time. In Fig. 5b, the slope of the line (equals to -1 /τ) shows the rate parameter. The rate of swelling and τ have an inverse relationship that means the lower the value of τ, the higher the swelling rate, which was used to evaluate the water absorption of nanohydrogels.

For comparison, SNN responds to swelling slower than DNN. Comparatively dense hydrogels with more effective drug loading and release can be formed by synthesizing DNNs [44-46]. It is also observed that the swelling equilibrium and rate of DNN are higher than those of SNN, and the swollen hydrogel improves the drug release [41]. According to Fig. 5b and using Equation 3, the rate parameter for SNN and DNN water swelling is 32.6 min and 27.5 min, respectively [32, 47]. This result is in agreement with studies by Pourjavadi et al. and authors' previous work, which showed that the obtained τ was 27 and 28 min, respectively [48, 49]. The similarity in the structures of entitled products could be the cause of this resemblance [48, 49].

UV-vis spectroscopy was used to investigate the release of DOX from the DNN structure under various conditions, including temperature, time, and pH.

Fig. 6a shows the release of DOX from DNN in PBS at pH values of 5.4, 7.4, and 9.0 at 25°C over 31 hours. Fig. 6a

shows that the amount of DOX released from the DNN was dependent on the pH of the solution. After 31 hours, the DOX release from the nanohydrogel in PBS with pH values of 5.4, 7.4, and 9.0 is 100%, 72% and 63%, respectively. As can be seen, the DOX release was increased significantly at phosphate buffer with a pH of 5.4 and 25°C. After 31 hours, 100% of the drug is released. This condition (pH 5.4, acidic pH) is like the environmental conditions of cancer cells [50, 51]. Due to the AA sensitivity to pH, the drug was released from the nanocarrier in buffer solutions with different pHs. This can be explained by the reduced DNN's swelling in an acidic environment, which leads to the drug being pushed out of the hydrogel system [52]. Also, partial loss of cross-linking by Ca^{2+} in an acidic condition may lead to partial breakdown of the network and thus cause more drug release under acidic conditions.

DOX release was also performed at 37°C and 45°C in PBS with pH 5.4. Fig. 6b shows that in pH 5.4 and in 21 hours, the release of DOX from the DNN is about 76% at 25°C, 93% at 37°C, and 100% at 45°C. At 25°C the interactions between the amine, carbonyl, and hydroxyl groups of DOX and DNN limit the conditions of release. The difference at 37°C and 45°C can be attributed to the reduction of interactions, such as hydrogen bonding, between the drug and the hydrophilic groups of DNN in these conditions [53, 54]. In the previous study, DOX release was examined at various pHs and temperatures. At pH 5.4 and 25°C, 60% of DOX was released in 25 hours, while at pH 5.4 and 41°C, 80% of DOX was released in 24 hours [30]. In this study, the results show that 60% of DOX was released at pH 5.4 and 25°C in 17 hours, and 80% of DOX was released at pH 5.4 and 45 °C in 16 hours, indicating the good performance of DNN as a nanocarrier. Both studies demonstrate that drug release increases with rising temperatures. Although drug release for DNN was performed in a shorter time under different conditions (temperature and pH).

Infrared spectroscopy was used to confirm the chemical structure of DNNs. In Fig. 7a–c, the raw materials spectra and their characteristic peaks are shown, and in Fig. 7d–g, the spectra of synthesized polymers are shown and discussed.

In Fig. 7a, the vibration of the C-H band at 980 cm^{-1} due to C=C-H (corresponding to AA) was shown. The characteristic peak of AA was attributed to C=C vibration was located at 1600 cm^{-1}. The peak at 1735 cm^{-1} was due to the asymmetric stretching vibrations of C=O in -COOH groups [55]. The broad peak at 3100-3500 cm^{-1} was related to the carboxylic acid functional group's O–H stretching [56].

In Fig. 7b, the peak at 1722 cm^{-1} was attributed to C=O stretching vibration and the peak at 1286 cm^{-1} was attributed to C-N stretching vibration [57]. The peaks between 1400 and 1492 cm^{-1} wavelengths correspond to the doxorubicin's aromatic ring. N-H vibrations were shown at 1605 cm^{-1} and 760 cm^{-1} [58].

In Fig. 7c, the vibration at 811 cm^{-1} is attributed to the Na–O bond in S-ALG. The band at 962 cm^{-1} was due to

the C-O stretching vibration of uronic acid residues. The vibrations at 1031 cm^{-1} and 1650 cm^{-1} can be attributed to the C-O and C=O groups, respectively. The band at 1607 cm^{-1} was attributed to the O-C-O carboxylate asymmetric stretching [59].

In Fig. 7d, the peak at 1600 cm^{-1} (corresponds to the C=C) was removed, which confirmed the successful synthesis of nanohydrogel. The band at the wavelength of 1720 cm^{-1} was ascribed to the stretching vibration of C=O in –COOH groups. When the alginate biopolymer was cross-linked through Ca^{2+} cations, the peak at 1607 cm^{-1} (corresponding to the COO$^-$ stretching peak in alginate) shifted to 1720 cm^{-1} in DNNs. The peak corresponding to CH$_2$- was displayed at 1472 cm^{-1}. The peaks at 2937 cm^{-1} and 2849 cm^{-1} correspond with the aliphatic C-H stretching bond, indicating the presence of aliphatic CH$_2$- groups in the structure and the formation of the polymer network. The vibration at 1500 cm^{-1} is attributed to stretching C–O bond [56, 60].

The corresponding DOX loaded DNN spectrum is shown in Fig. 7e. The presence of DOX in the DNN structure is confirmed by the characteristic peak at 760 cm^{-1}, which corresponds to N-H bending vibration in DOX, as shown. Also, the peak at 1492 cm^{-1}, which corresponds to the aromatic ring of DOX, was visible more strongly. C-N stretching vibration appeared at 1286 cm^{-1} [57]. The broad peak related to the O-H stretching vibrations at 3300-3600 cm^{-1} in the DNN structure overlapped with the N-H stretching vibrations in the DOX loaded DNN structure. The spectrum shows the successful DOX loading onto the DNN structure [51].

After drug release, in Fig. 7f, the peak at 760 cm^{-1} corresponding to the N-H bending vibration of DOX and the vibration at 1286 cm^{-1} due to the C-N stretching vibration appeared diminished, indicating that the drug release from DNN was well done.

The SNN spectrum is shown in Fig. 7g, which demonstrates all the characteristic peaks and indicates the successful synthesis of SNN.
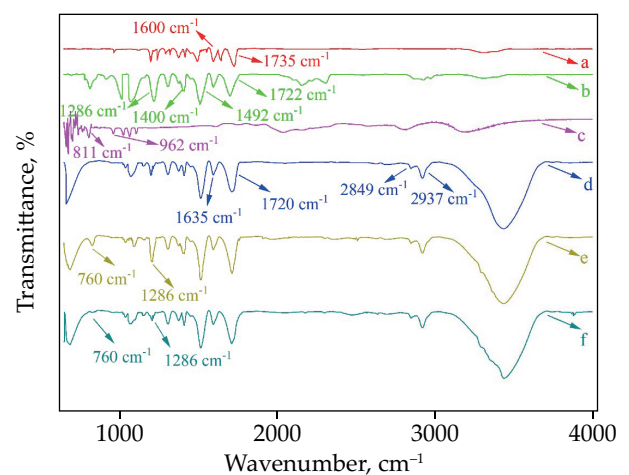

Fig. 7. Infrared spectra: a) AA, b) DOX, c) S-ALG, d) DNN, e) DOX loaded DNN, f) DNN after DOX release, g) SNN
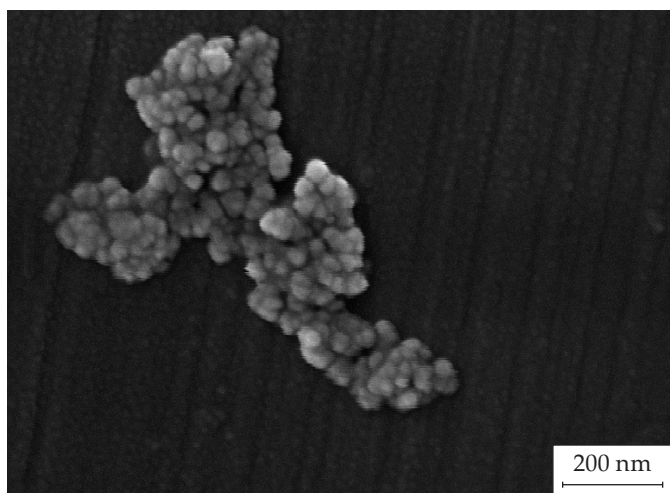
Fig. 8. SEM image of DOX loaded DNN

SEM image was used to determine the morphological properties of DOX loaded DNN. As can be seen in Fig. 8, they are spherical. According to SEM results, DNNs have an average size of 10-20 nm [56].

The DLS technique was used to determine the particle size distribution and zeta potential for SNN and DNNs, as shown in Fig. 9a–c. Particle size and charge are two major factors that could play key roles in drug delivery systems. The body has several barriers that limit the absorption and circulation of drug carriers. Two of these factors include the size of the drug carrier particles and their surface charge, which influence the drug carriers' distribution and their interactions with cells [61]. Neutrally charged nanoparticles (with zeta potential values of approximately −10 to +10 mV) exhibit better delivery efficiencies than nanoparticles with higher zeta potential. In addition, particles with a hydrodynamic diameter of less than 100 nm have greater delivery efficiencies than larger ones [62, 63].

After the synthesis of SNN and DNNs in the organic/aqueous reaction mixture, they were sonicated in an ultrasonic bath for 5 min, and then they passed through a syringe filter (pore size: 0.2 μm) and were used for DLS. The process of measuring zeta potential involves dispersing nanoparticles in a liquid medium in cell while applying an electric field (generated by two electrodes). The oppositely charged particles approach the electrodes at a rate determined by their electrophoretic mobility as soon as a voltage is applied to the electrodes. The zeta potential of dispersed nanoparticles is related to their electrophoretic mobility (μ_{ep}) according to Henry's equation (Equation 5) [64].

$$\mu_{ep} = \frac{2\,d \cdot z \cdot f\,(ka)}{3\,\eta} \qquad (5)$$

where d is the dielectric constant, z is the zeta potential, f (ka) is Henry's function (f (ka): 1.5) and η is the viscosity of the dispersing environment [51].

The zeta potentials of SNN, DNN and DOX loaded DNN are -0.7, -0.6 and -0.1 mV, respectively. The presence

of DOX in DNNs caused the surface charge to decrease to -0.1 mV, which decreased the repulsive force between the nanoparticles. As a result, as seen in Fig. 9c, larger-sized nanoparticles relative to the pristine nanohydrogel were produced [56, 65]. The particle sizes of SNN, DNN, and DOX loaded DNN were measured by DLS 9 nm, 8 nm, and 10 nm, respectively. In DLS, hydrodynamic size is measured. In this study, due to the presence of the samples in the organic/aqueous solvent, the DNNs did not show a sizeable hydrodynamic diameter, for this reason, there is no significant sizes difference between the SEM and DLS images.

The TGA method was used to show the thermal behavior of the synthesized DNNs. This is a common method for evaluating the polymer's thermal stability at various temperatures. The thermal behavior at high temperatures was investigated to characterize and demonstrate that the polymer's thermal behavior is unchanged following drug loading in the nanohydrogel, and that the polymer structure is preserved up to temperatures exceeding 100°C. For these reasons, the TGA curves are demonstrated at the temperature range of 25–700°C (Fig. 10a).
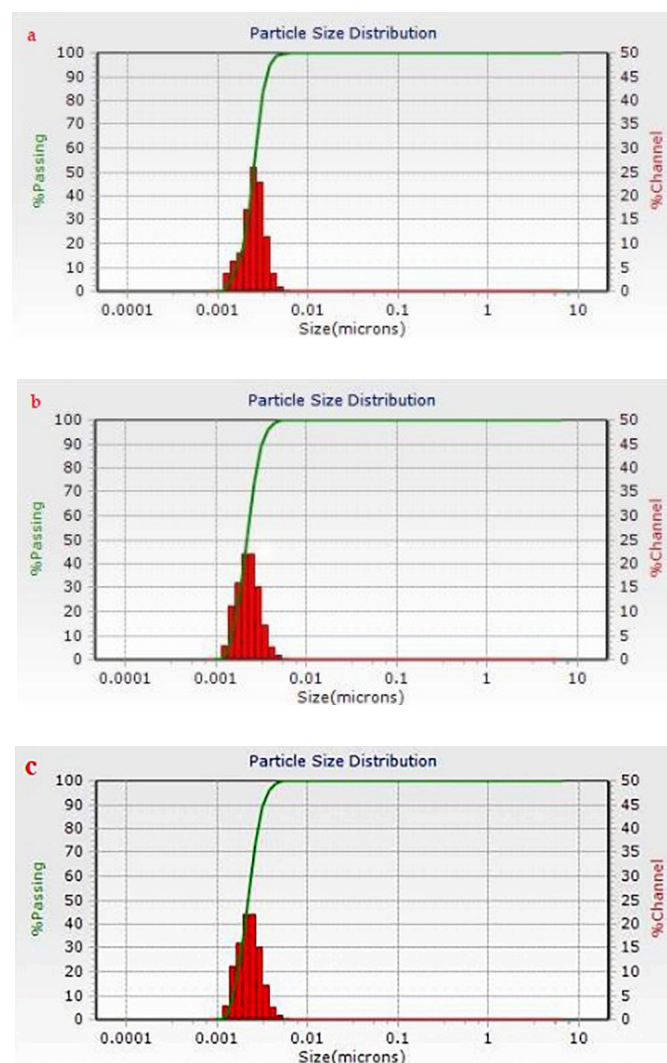

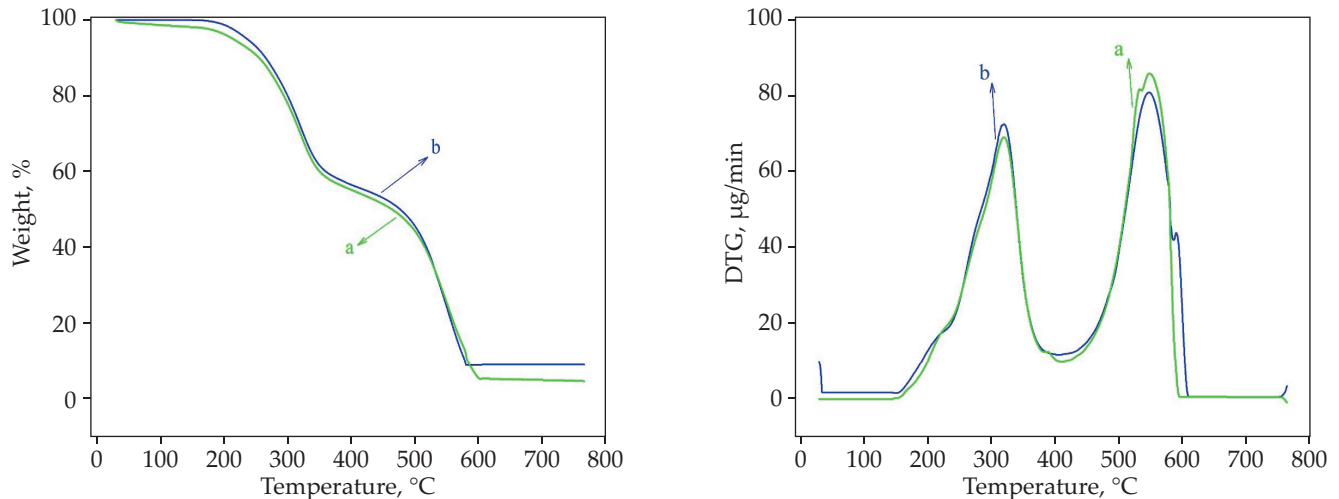**Fig. 9. Particle size distribution: a) SNN, b) DNN, c) DOX loaded DNN**

Fig. 10. Thermogravimetric curves of DNN: a) TG, b) DTG

The TGA and DTG diagrams show thermal degradation that is typically associated with the breaking of polysaccharide chains, monomers and network connections [66, 67]. The difference in thermal decomposition is seen in the DTG diagram of two DNNs. The DTG diagram confirms the decomposition of DNNs and shows the start and end temperatures of degradation. As shown in Fig. 10a and b, two DNNs have two distinct degradation stages. In the first step breaking of C-O bonds in the chains of polymers occurs, simultaneously to the breakdown of the pyranose rings. This phenomenon can be seen in the weight loss of the first step of decomposition between 198°C and 310°C. The second step of decomposition between 310°C and 554°C can be attributed to the degradation of the poly(acrylic acid) structure [30]. As can be seen in Fig. 10a and b, there is no significant difference in the thermal stability between the two nanohydrogels. Two degradation steps with an 88% weight loss occurred in the case of DOX loaded DNN [67, 68].

The nanohydrogel carrier is used for drug release, and the release process is usually performed at a physiological temperature of 37°C. Form Fig. 10a can be concluded, that the DOX loaded DNN is completely stable in the environment at 37°C. The maximum temperature (T_{max}) is an important factor in determining the thermal stability of a thermal degradation process. T_{max} is the temperature derived from the TGA diagram that indicates the maximum degradation of the polymer and the maximum weight loss. An increase in T_{max} indicates a rise in the thermal stability of a polymer, and the thermal behavior of DOX loaded DNN shows almost the same performance with DNN [67, 69]. Table 2 shows the thermal degradation temperatures (T_{onset}, $T_{5\%}$, and T_{max}) and ash content of DNNs.

CONCLUSIONS

This study describes the synthesis and characterization of DOX loaded DNN based on poly(acrylic acid) grafted on S-ALG as a biocompatible polymer via inverse miniemulsion polymerization. Also, to demonstrate the advantages of DNN in drug delivery systems, the results were compared with those of SNN and non-nanogel systems, and the results showed the good performance of DNN.

For the synthesis of DNN, several factors were studied and optimized, including AA, MBA, and APS (AA: 120 µl, MBA: 13.2 µl (2.5% w/v), APS: 16.7 µl (2.5% w/v)) and under these conditions, the maximum water absorbency was determined to be 250 g/g. The synthesis of DNN and DOX loaded DNN was confirmed by FT-IR. The spectra show that DNN has been properly synthesize, DOX was appropriately loaded onto the DNN structure, and the drug was successfully released from the DNN structure. According to the TGA, the first stage of decomposition occurred between 198°C and 310°C and the second stage occurred between 310°C and 554°C. It was observed that the thermal stability of DOX loaded DNN is like that of DNN. DLS was used to measure the particle size and zeta potential, and the results demonstrated the appropriate conditions for effective drug delivery. SEM was used for observing the surface morphology of the spherical DOX loaded DNN. DNN demonstrated a good equilibrium swelling capacity in water as a nanohydrogel drug carrier in drug delivery system, and the swelling kinetic equation was used to determine the DNN rate parameter (27.54 min). UV spectroscopy was used to study the rate of DOX release under various environmental conditions, including pH and temperature. After 21 hours at pH 5.4 and 45°C, and after 31 hours at pH 5.4 and 25°C, 100% of the

T a b l e 2. Degradation temperature of DNNs

Samples	T_{onset} °C	$T_{5\%}$ °C	T_{max} °C	Ash content, %
DOX loaded DNN	203.1	215.6	554.5	5.2
DNN	198.3	205.9	540.2	3.6

DOX had been released into the environment. Due to the similarity of this condition (pH 5.4) with the environment of cancer cells, it may be concluded that the synthesis of DNNs responsive to pH and temperature can be considered as a candidate for improving drug delivery systems.

Authors contribution

G.R.B. – Conceptualization, Funding acquisition, Project administration, Resources, Supervision, Validation; M.N. – Methodology, Validation, Investigation, Data curation, Formal analysis, Funding acquisition, Writing; K.D. – Supervision, Validation.

Funding

Conflict of interest

The authors have no conflicts of interest to declare.

REFERENCES

[1] Sethi S., Thakur S., Singh A. *et al.:* "Biopolymeric Nanohydrogels as Devices for Controlled and Targeted Delivero of Drugs" in "Green and Sustainable Nanotechnology: Fundamentals, Developments and Applications", Springer, Cham 2023. p. 1857.
https://doi.org/10.1007/978-3-031-16101-8_69

[2] Gao Y., Vogus D., Zhao Z. *et al.: Bioengineering and Translational Medicine* **2021**, *7(1)*, 10245.
https://doi.org/10.1002/btm2.10245

[3] Rajput R., Narkhede J., Naik J.: *ADMET and DMPK* **2020**, *8(1)*, 1.
https://doi.org/10.5599/admet.724

[4] Li C., Obireddy S.R., Lai W.F.: *Drug Deliv* **2021**, *28(1)*, 1594.
https://doi.org/10.1080/10717544.2021.1955042

[5] Altuntaş E., Özkan B., Güngör S. *et al.: Pharmaceutics* **2023**, *15(6)*, 1644.
https://doi.org/10.3390/pharmaceutics15061644

[6] Martău G.A., Mihai M., Vodnar D.C.: *Polymers* **2019**, *11(11)*, 1837.
https://doi.org/10.3390/polym11111837

[7] Szabó L., Gerber-Lemaire S., Wandrey C.: *Polymers (Basel)* **2020**, *12(4)*, 919.
https://doi.org/10.3390/polym12040919

[8] Butowska K., Woziwodzka A., Borowik A. *et al.:. Materials (Basel)* **2021**, *14(9)*, 2135.
https://doi.org/10.3390/ma14092135

[9] Thorn C. F., Oshiro C., Marsh S. *et al.: Pharmacogenetics Genomics* **2011**, *21(7)*, 440.
https://doi.org/10.1097/FPC.0b013e32833ffb56

[10] Vyas M., Simbo A. D., Mursalin M. *et al.: Current Cancer Therapy Reviews* **2020**, *16(4)*, 320.
https://doi.org/10.2174/1573394716666191216114950

[11] Lakkakula J.R., Gujarathi P., Pansare P. *et al.: Carbohydrate Polymers* **2021**, *259*, 117696.
https://doi.org/10.1016/j.carbpol.2021.117696

[12] Kamenova K., Radeva L., Yoncheva K. *et al.: Polymers* **2022**, *14(17)*, 3694.
https://doi.org/10.3390/polym14173694

[13] Qiu Y., Park K.: *Advanced Drug Delivery Reviews* **2001**, *53(3)*, 321.
https://doi.org/10.1016/S0169-409X(01)00203-4

[14] Sharpe L.A., Daily A.M., Horava S.D. *et al.: Expert Opin Drug Delivery* **2014**, *11(6)*, 901-15.
https://doi.org/10.1517/17425247.2014.902047

[15] Li L., Wu P., Yu F. *et al.: Journal of Materials Chemistry A* **2022**, *17(10)*, 9215.
https://doi.org/10.1039/D2TA00540A

[16] Zhuang, Y., Kong Y., Han K. *et al.: New Journal of Chemistry* **2017**, *41(24)*, 15127.
https://doi.org/10.1039/C7NJ03392C

[17] Ning X., Hung J., Yuan N. *et al.: International Journal of Molecular Sciences* **2022**, *23(24)*, 15757.
https://doi.org/10.3390/ijms232415757

[18] Huang X., Li J., Luo J. *et al.: Materials Today Communications* **2021**, *29*, 102757.
https://doi.org/10.1016/j.mtcomm.2021.102757

[19] Fan Z., Ji D., Kim J.: *Advanced Intelligent System* **2023**, *5(10)*, 2300194.
https://doi.org/10.1002/aisy.202300194

[20] Chen K., Liu M., Wang F. *et al.: Frontiers in Bioengineering and Biotechnology* **2022**, *10*, 198.
https://doi.org/10.3389/fbioe.2022.846401

[21] Pourjalili N., Bagheri Marandi G.B., Kurdtabar M. *et al.: Polymers for Advanced Technologies* **2023**, *34(4)*, 1315.
https://doi.org/10.1002/pat.5972

[22] Pourjalili N., Marandi G.B., Kurdtabar M. *et al.: Journal of Macromolecular Science, Part A* **2022**, *59(8)*, 537.
https://doi.org/10.1080/10601325.2022.2092411

[23] Surikutchi B.T., Obenza-Otero R., Russo E. *et al.: International Journal of Pharmaceutics* **2022**, *622*, 121828.
https://doi.org/10.1016/j.ijpharm.2022.121828

[24] Zhang H., Shi L.W.E., Zhou J.: *Journal of Polymer Science* **2023**, *61(1)*, 7.
https://doi.org/10.1002/pol.20220510

[25] Zeng L., He J., Cao Y. *et al.: Smart Materials in Medicine* **2021**, *2*, 229.
https://doi.org/10.1016/j.smaim.2021.07.005

[26] Asua J.M.: *Progress in Polymer Science* **2002**, *27(7)*, 1283.

[27] Faucheu J., Gauthier C., Chazeau L. *et al.: Polymer* **2010**, *51(1)*, 6.
https://doi.org/10.1016/j.polymer.2009.11.044

[28] Thakur S., Sharma B., Verma A. *et al.: Journal of Cleaner Production* **2018**, *198*, 143.
https://doi.org/10.1016/j.jclepro.2018.06.259

[29] Sevinç-Özakar R., Seyret E., Özakar E. *et al.: Gels* **2022**, *8(9)*, 578.
https://doi.org/10.3390/gels8090578

[30] Rezanejade Bardajee G., Ghadimkhani R., Jafarpour F.: *International Journal of Biological Macromolecules* **2024**, *260(2)*, 128871.
https://doi.org/10.1016/j.ijbiomac.2023.128871

[31] Guo, B., Liang Y., Dong R.: *Nature Protocols* **2023**, *18(11)*, 3322.
https://doi.org/10.1038/s41596-023-00878-9

[32] Rezanejade Bardajee G., Mizani F., Hosseini S.S.: *Journal of Polymer Research* **2017**, *24(3)*, 48.
https://doi.org/10.1007/s10965-017-1197-4

[33] Suhail M., Liu J.-Y., Khan A. *et al.: Journal of Materials Research and Technology* **2022**, *19*, 3073.
https://doi.org/10.1016/j.jmrt.2022.06.056

[34] Andreazza R., Morales A., Pieniz S. *et al.: Polymers* **2023** *15(4)*, 1026.
https://doi.org/10.3390/polym15041026

[35] Ahmed E.M.: *Journal of Advanced Research* **2015**, *6(2)*, 105.
https://doi.org/10.1016/j.jare.2013.07.006

[36] Li J., Zhang L., Gu J. *et al.: RSC Advances* **2015,** *5(26)*, 19859.
https://doi.org/10.1039/C4RA15482G

[37] Nasution H., Harahap H., Dalimunthe N.F. *et al.: Gels* **2022**, *8(9)*, 568.
https://doi.org/10.3390/gels8090568

[38] Sadeghi M., Heidari B.: *Materials (Basel)* **2011**, *4(3)*, 543.
https://doi.org/10.3390/ma4030543

[39] Chen J., Zhao Y.: *Journal of Applied Polymer Science* **2000**, *75(6)*, 808.
https://doi.org/10.1002/(SICI)1097-4628(20000207)75:6<808::AID-APP10>3.0.CO;2-3

[40] Wang W.B., Wang A.Q.: *Advanced Materials Research* **2010**, *96*, 177.
https://doi.org/10.4028/www.scientific.net/AMR.96.177

[41] Lee C.S., Hwang H.S.: *Gels* **2023**, *9(12)*, 951.
https://doi.org/10.3390/gels9120951

[42] Schott H.: *Journal of Pharmaceutical Sciences* **1992**, *81(5)*, 467.
https://doi.org/10.1002/jps.2600810516

[43] Ghobadifar V., Bagheri Marandi G., Kurdtabar M. *et al.: Iranian Journal of Chemistry and Chemical Engineering* **2023**, *42(3)*, 875.

[44] Dragan E.S.: *Chemical Engineering Journal* **2014**, *243*, 572.
https://doi.org/10.1016/j.cej.2014.01.065

[45] Dragan E. S.: *Pure and Applied Chemisty* **2014**, *86(11)*, 1707.
https://doi.org/10.1515/pac-2014-0713

[46] Myung, D., Waters D., Wiseman M. *et al.: Polymers for Advanced Technologies* **2008,** *19(6)*, 647.
https://doi.org/10.1002/pat.1134

[47] Sadeghi M., Hosseinzadeh H.: *Journal of Applied Polymer Science* **2008**, *108(2)*, 1142.
https://doi.org/10.1002/app.26464

[48] Pourjavadi A., Ghasemzadeh H., Hosseinzadeh H.: *e-Polymers* **2004**, *4*, 027.
https://doi.org/10.1515/epoly.2004.4.1.275

[49] Rezanejade Bardajee G., Sharifi M., Torkamani H. *et al.: Colloids and Surfaces A: Physicochemical and Engineering Aspects* **2021**, *616*, 126350.
https://doi.org/10.1016/j.colsurfa.2021.126350

[50] Cao Z., Li W., Liu R. *et al.: Biomedicine and Pharmacotherapy* **2019**, *118*, 109340.
https://doi.org/10.1016/j.biopha.2019.109340

[51] Pethő Z., Najder K., Carvalho T. *et al.: Cancers (Basel)* **2020**, *12(9)*, 2484.
https://doi.org/10.3390/cancers12092484

[52] Mao J., Kondu S., Ji H.-F. *et al.: Biotechnology and Bioengineering* **2006**, *95(3)*, 333.
https://doi.org/10.1002/bit.20755

[53] Dadsetan M., Taylor K.E., Yong C. *et al.: Acta Biomaterialia* **2013**, *9(3)*, 5438.
https://doi.org/10.1016/j.actbio.2012.09.019

[54] Farjadian F., Rezaeifard S., Naeimi M. *et al.: International Journal of Nanomedicine* **2019**, *14*, 6901.
https://doi.org/10.2147/IJN.S214467

[55] Elbayomi S.M., Wang H., Tamer T.M. *et al.: Polymers* **2021**, *13(15)*, 2575.
https://doi.org/10.3390/polym13152575

[56] Aminoleslami D., Porrang S., Vahedi P. *et al.: Oxidative Medicine and Cellular Longevity* **2022**, *1*, 1548410.
https://doi.org/10.1155/2022/1548410

[57] Ya-zhen W., Xue-ying W., Yu-tao D. *et al.: Journal of Nanomaterials* **2020**, *1*, 5492953.

[58] Lungu I.I., Nistorescu S., Badea M. A. *et al.: Polymers* **2020**, *12(12)*, 2799.
https://doi.org/10.3390/polym12122799

[59] Belattmania Z., Kaidi S., El Atouani S. *et al.: Molecules* **2020**, *25(18)*, 4335.
https://doi.org/10.3390/molecules25184335

[60] Rezanejade Bardajee G., Asgari S., Mirshokraie S. A.: *Iranian Journal of Chemistry and Chemical Engineering* **2021**, *40(5)*, 1386.

[61] Di J., Gao X., Du Y. *et al.: Asian Journal of Pharmaceutical Sciences* **2021**, *16(4)*, 444.
https://doi.org/10.1016/j.ajps.2020.07.005

[62] Niroumand U., Firouzabadi N., Goshtasbi G. *et al.: Frontiers in Materials,* **2023**, *10*, 1189463.
https://doi.org/10.3389/fmats.2023.1189463

[63] Oyewumi M. O., Kumar A., Cui Z.: *Expert Review of Vaccines* **2010**, *9(9)*, 1095.
https://doi.org/10.1586/erv.10.89

[64] Varenne F., Botton J., Merlet C. *et al.: Colloids and Surfaces A: Physicochemical and Engineering Aspects* **2015**, *486*, 218.
https://doi.org/10.1016/j.colsurfa.2015.08.044

[65] Alshawwa S.Z., Kassem A.A., Farid R.M. *et al.: Pharmaceutics* **2022**, *14(4)*, 883.
https://doi.org/10.3390/pharmaceutics14040883

[66] Kołodyńska D., Skiba A., Górecka B. *et al*.: "Hydrogels from Fundaments to Application" in "Emerging Concepts in Analysis and Applications of Hydrogels", IntechOpen, Rijeka 2016, p. 69.
https://dx.doi.org/10.5772/63466

[67] Flores-Hernández C.G., Cornejo-Villegas M.L.A., Moreno-Martell A. *et al.: Polymers* **2021**, *13(4)*, 504.
https://doi.org/10.3390/polym13040504

[68] Nurazzi N.M., Asyraf M.R.M., Rayung M. *et al.: Polymers* **2021**, *13(16)*, 2710.
https://doi.org/10.3390/polym13162710

[69] Zhang Y., Wang Q., Wang Z. *et al.: ChemPlusChem* **2021**, *86(11)*, 1524.
https://doi.org/10.1002/cplu.202100474